Gas Bubble Shape Measurement and Analysis

Claudius Zelenka

Institute of Computer Science, Kiel University, Germany

Abstract. This work focuses on the precise quantification of bubble streams from underwater gas seeps. The performance of the snake based method and of ellipse fitting with the CMA-ES non-linear optimization algorithm is evaluated. A novel improved snake based method is presented and the optimal choice of snake parameters is studied. A Kalman filter is used for bubble tracking. The deviation between the measured flux and a calibrated flux meter is 4% for small and 9% for larger bubbles. This work will allow a better data gathering on marine gas seeps for future climatology and marine research.

1 Introduction

Underwater gas seeps have essential influence on marine life [6] and global climate [12]. Modeling and understanding of their complex impacts on the biosphere requires exact knowledge of the composition and volume of the emitted gases and their absorption in the surrounding water [13].
Gas bubbles emerging from a seep in the sea floor are rising with high speed, and may change form, contour and volume during their ascent [4]. The goal of this research is the development of robust methods for automatic image processing, which can be employed to extract the shape, motion and volume of bubbles from image sequences.

The first part of this paper is dedicated to the detection of gas bubbles. Several methods are compared, the snake [8] approach and ellipse fitting with the CMA-ES [5] non-linear optimization algorithm. Diffuse back light illumination is used, in a similar configuration as in previous work by [10], [11], or [15].

For the detection of bubbles different detection methods are established in previous work. In [2] active contours are initialized using the boundaries of the binarized input image. Another approach, presented in [3] uses a specialized Hough transformation on the input image to locate the circular or ellipsoid shape of bubbles. In [14] the application of a Canny edge detector [1] for contour extraction is presented. These contours are fitted and smoothed with an ellipse. In this work the Canny edge detection according to this publication [14] is used as a baseline method. On this basis, methods and algorithms based on the standard and improved snake algorithm are developed and evaluated. The CMA-ES based ellipse fitting method with diverse novel fitness functions is in

Recommended for submission to YRF2014 by Prof. Dr.-Ing. Reinhard Koch, Kiel University.

this work extensively studied. The results are compared with manual ground truth evaluation of the bubble size.

In the second part of this work, methods for the tracking of bubbles and measuring of their velocity are developed. The accuracy of the detection and tracking methods in combination are verified by comparison with manually obtained flux data. Figure 1 illustrates the typical irregular bubble shapes and the bubble matching.

(a) Frame 1 (b) Frame 2 (c) Combined

Fig. 1. Movement of bubbles in between two frames at 100fps. The combination shows frame 1 and 2 with the bubble detection in frame 2 in red and matching bubbles connected in green.

2 Bubble Detection

In this section methods for the reliable detection of bubble contour in image sequences are developed. The Canny Edge detector based method by [14] is used as a baseline. It sporadically suffers from false detections, which motivates the search for more stable algorithms. These false detections are caused by the light area inside the bubble. As an improvement a bounding box is formed around these detections and expanded. This bounding box is used as an initialization for the snake [8] and CMA-ES [5] based methods, which are introduced, tested and evaluated in the following.

2.1 Snake Method

The term snake was coined by Kass et al. in [8] and describes a spline, which is adjusted by the snake method to fit a prior defined criterion. For every contour, an energy function is declared. It can be described in two parts, the internal

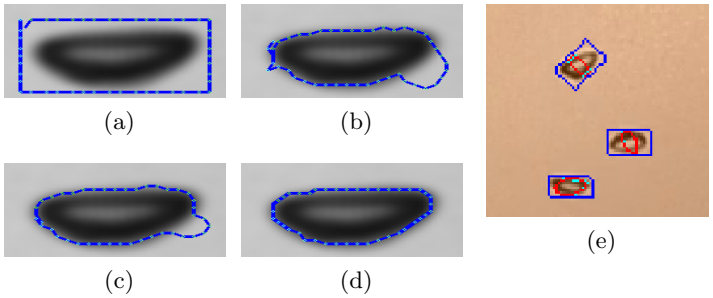

Fig. 2. Subfigures (a) to (d) show steps in the optimization process of the classic snake algorithm, from initialization to termination. The control points are depicted in green, while the linear interpolation in between them is shown in blue. Subfigure (e) shows an imperfect detection with the classic snake algorithm on an image with low image quality.

energy E_{int}, weighted with α and β, which is dependent purely on the snake's shape, and the external energy E_{ext}. Let $S : M \to P$ be a snake, with $M = [0, 1]$ and $P \subset \mathbb{R}^2$ for all points on the snake. Let S_{final} be the optimal configuration of the snake:

$$S_{final} = arg\,min(E_{int}(S) + E_{ext}(S))\,. \tag{1}$$

$$E_{int}(S) = \int_0^1 \alpha \left\|S'(c)\right\|^2 + \beta \left\|S''(c)\right\|^2 \mathrm{d}c\,. \tag{2}$$

The external energy is used to describe the part of the energy, which depends on the image signal. It is weighted with parameter γ. Given image $I : [0, x] \times [0, y] \to \mathbb{R}^+$ with width $x \in \mathrm{Z}^+$ and height $y \in \mathrm{Z}^+$, it holds that:

$$E_{ext}(S) = \int_0^1 -\gamma \left\|\nabla I(S(c))\right\|^2 \mathrm{d}c\,. \tag{3}$$

The snake contour is initialized with the bounding box from the baseline localization. Figure 2 shows different iterations of a succesful localization of a bubble with a snake, from initialization to convergence.

The choice of snake parameters α, β and γ, which control the snakes affinity to continuity, low curvature and high gradients have significant impact on the convergence behaviour of snakes. An important question, which is not sufficiently adressed in previous work, concerns the optimum choice of snake parameters. In this work extensive investigation is done to find out, whether the snake parameters can stay constant, or must be adapted to each bubble stream, or perhaps to each bubble. The entire parameter space of α,β and γ has been tested with different bubble sequences. It was shown, that if α is high enough, then the parameters choice is not critical and the same optimized set of parameters can be used for different bubble streams, even from different cameras.

2.2 Gradient Snake Method

Figure 2(e) shows an example of a bubble in an low quality image sequence, on which the classic snake approach seems not to work reliably due to light area in the centre of the bubble, which causes areas with high gradients inside the bubble. Therefore, a novel enhancement of the snake method is proposed, which improves the detection of such bubbles, as can be seen in Figure 3(e). The concept of the new gradient snake approach is shown on Figure 3, in which different steps of the snake algorithm with the novel term are shown with the image gradient vector depicted in green hues and contour normal vector in lilac hues. They illustrate the effectiveness of the novel term particularly for the detection of bubbles.

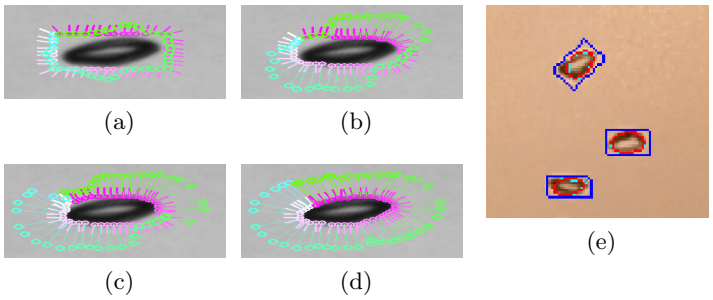

Fig. 3. Subfigures (a) to (d) show every third step in the optimization process of the snake algorithm with directional gradient, from initialization to termination. Lilac hues show the normal of the contour, green hues show the direction and magnitude of the gradient indicated by the length of the greenish indicators. Subfigure (e) shows the detection with the gradient snake algorithm on the same input image as Figure 2(e).

At position c, the dot product is applied to the image gradient and the outwards normal $\widehat{n}$ of the contour. If they point in the same direction, the result is positive and if they point in different directions it is negative. The result is scaled with the squared absolute value of the image gradient and is similar to E_{ext} weighted with parameter γ. For the following applies:

$$E_{gd}(S) = \int_0^1 -\gamma \left\langle \frac{\nabla I(S(c))}{\|\nabla I(S(c))\|}, \widehat{n}(S(c)) \right\rangle \|\nabla I(S(c))\|^2 \,\mathrm{d}c\,. \tag{4}$$

Using the sum of the normal and gradient direction vectors, instead of the dot product, has the advantage of gaining linear sensitivity to an angular difference between $\widehat{n}$ and $\nabla S(c)$ over the *cosine* and lower computational complexity. The difference is then scaled by 0.5 to achieve values, which are in the same scale as the original snake algorithm, for coinciding vectors:

$$E_{gd}(S) = \int_0^1 -0.5\,\gamma \left\| \frac{\nabla I(S(c))}{\|\nabla I(S(c))\|} + \widehat{n}(S(c)) \right\| \|\nabla I(S(c))\|^2 \mathrm{d}c\,. \tag{5}$$

2.3 CMA-ES Based Ellipse Fitting

Covariance Matrix Adaption - Evolution Strategy (CMA-ES) is a derivative free non-linear optimization algorithm [5]. For the detection of gas bubbles the algorithm is initialized with the expanded bounding box of the Canny edge detection, as described in Section 2. The CMA-ES algorithm then adjusts an ellipse to the bubble, according to a prior defined fitness function. The ellipse used in the optimization is defined by five parameters, the horizontal and vertical position of the bubble, its minor and major axis and a rotation parameter. Different fitness functions have been developed and tested. Two designs showed the best results, firstly a fitness function aiming for a high gradient on the edge of the ellipse and secondly an area based fitness function evaluating the difference between the mean intensities of the ellipse area and its surroundings.

2.4 Comparison of Detection Methods

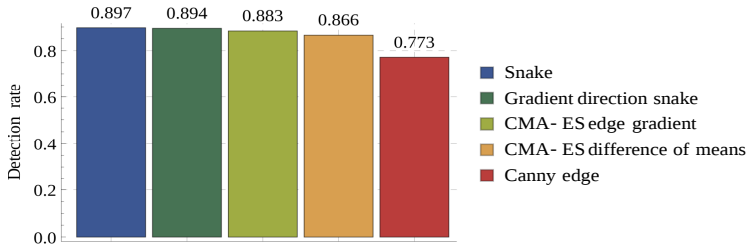

Fig. 4. Comparison of detection rates for several selected methods on an high quality GoPro image sequence with manual ground truth on 20 images.

In Figure 4 the detection rates of different methods are compared with manual ground truth for an image sequence of 20 images with ca. 10 bubbles visible per frame. All tested methods show good results and a clear improvement compared to the baseline Canny edge detector, however both snake based methods showed the best performance. The fastest method is the classic snake algorithm with timings of about 30ms per frame. Even though it is slower, being most reliable on images with low image quality (see Figure 3(e)), the gradient direction snake has been determined as the bubble detection method of choice.

3 Bubble Tracking

Bubble tracking is employed to determine the movement of bubbles in between two frames and from this data over the entire image sequence. To effectively find the corresponding bubble detections between two frames, the bubble positions are detected in every frame. The bubble motion since the last frame is

predicted using a Kalman filter [7]. These predictions and the new detections of bubble positions are matched with minimum weighted matching between prediction and measurement using the hungarian algorithm [9], with the distances between these as edge weights. This resulting matching is the mapping of bubble movement between the last frame and this frame. A resulting matching is shown in Figure 1 on the right image. In the tested 20 sequences, with a bubble detection rate according Figure 4, the tracking is highly reliable. For a sequence such as Figure 1, the framerate can be lowered by 50% without deteriorating the tracking quality.

4 Conclusion

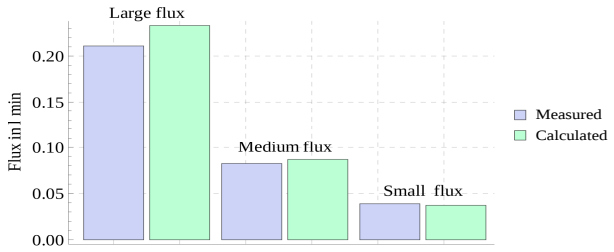

Fig. 5. Comparison between measured and calculated flux in liter per minute.

With the established methods for detecting and tracking bubbles, an accurate measurement of the flow volume from images of bubble stream can be done with high accuracy for wide range of flux volume, as shown in Figure 5. The computed flux data has been compared with flux volume obtained by independent measurement with a calibrated volume flux meter. With small bubbles a very good accuracy of 4% deviation can be achieved, for medium bubbles the deviation is 5% and for larger bubbles the deviation is higher with 9%. This can be explained by the rather irregular shape of larger bubbles.

It has been shown, that the snake method and the CMA-ES method are well suited for flux measurement of gas bubble seeps. The stability and performance of both methods was explored and improved.

5 Acknowledgements

This work was supported by the University of Kiel and GEOMAR Helmholtz Centre for Ocean Research Kiel. I am also grateful for support from Prof. Dr.-Ing. Reinhard Koch and Dr. Anne Jordt for my work.

References

1. Canny, J.: A computational approach to edge detection. IEEE Transactions on Pattern Analysis and Machine Intelligence PAMI-8(6), 679–698 (1986)
2. Cheng, D.c., Burkhardt, H.: Bubble recognition from image sequences. Proceedings of Eurotherm Seminar 68, Inverse problems and experimental design in thermal and mechanical engineering (2001)
3. Goulermas, J.Y., Liatsis, P.: Novel combinatorial probabilistic hough transform technique for detection of underwater bubbles. vol. 3029, pp. 147–156 (1997)
4. Greinert, J., Artemov, Y., Egorov, V., Debatist, M., Mcginnis, D.: 1300-m-high rising bubbles from mud volcanoes at 2080m in the black sea: Hydroacoustic characteristics and temporal variability. Earth and Planetary Science Letters 244(1-2), 1–15 (Apr 2006)
5. Hansen, N., Kern, S.: Evaluating the CMA evolution strategy on multimodal test functions. In: Parallel Problem Solving from Nature - PPSN VIII, vol. 3242, pp. 282–291. Springer Berlin Heidelberg, Berlin, Heidelberg (2004)
6. Ishimatsu, A., Kikkawa, T., Hayashi, M., Lee, K.S., Kita, J.: Effects of CO2 on marine fish: Larvae and adults. Journal of Oceanography 60(4), 731–741 (2004)
7. Kalman, R.: A new approach to linear filtering and prediction problems. Transactions of the ASME Journal of Basic Engineering (82 (Series D)), 35–45 (1960)
8. Kass, M., Witkin, A., Terzopoulos, D.: Snakes: Active contour models. International journal of computer vision 1(4), 321331 (1988)
9. Kuhn, H.W.: The hungarian method for the assignment problem. Naval Research Logistics Quarterly 2(1-2), 83–97 (Mar 1955)
10. Leifer, I., De Leeuw, G., Cohen, L.H.: Optical measurement of bubbles: System design and application. Journal of atmospheric and oceanic technology 20(9), 13171332 (2003)
11. Leifer, I., de Leeuw, G., Kunz, G., H. Cohen, L.: Calibrating optical bubble size by the displaced-mass method. Chemical Engineering Science 58(23-24), 5211–5216 (Dec 2003)
12. Lelieveld, J., Crutzen, P.J., Dentener, F.J.: Changing concentration, lifetime and climate forcing of atmospheric methane. Tellus B 50(2), 128–150 (Apr 1998)
13. McGinnis, D.F., Greinert, J., Artemov, Y., Beaubien, S.E., West, A.: Fate of rising methane bubbles in stratified waters: How much methane reaches the atmosphere? Journal of Geophysical Research 111(C9) (2006)
14. Thomanek, K., Zielinski, O., Sahling, H., Bohrmann, G.: Automated gas bubble imaging at sea floor; a new method of in situ gas flux quantification. Ocean Science 6(2), 549–562 (Jun 2010)
15. Wang, H., Dong, F.: Image features extraction of gas/liquid two-phase flow in horizontal pipeline by GLCM and GLGCM. pp. 2–135–2–139. IEEE (Aug 2009)